Resolving subcycle electron emission in strong-field sequential double ionization

Aihong Tong,[1,2] **Yueming Zhou,**[1,*] **and Peixiang Lu,**[1,3]

[1]*Wuhan National Laboratory for Optoelectronics and School of Physics, Huazhong University of Science and Technology, Wuhan 430074, China*
[2]*Department of Physics and Mechanical and Electrical Engineering, Hubei University of Education, Wuhan 430205, China*
[3]*Laboratory of Optical Information Technology, Wuhan Institute of Technology, Wuhan 430073, China*
[*]*zhouymhust@hust.edu.cn*

Abstract: Using a fully classical model, we have studied sequential double ionization (SDI) of argon driven by elliptically polarized laser pulses at intensities well in the over-barrier ionization region. The results show that ion momentum distributions evolve from the two-band structure to the four-band, six-band structure and finally to the previously obtained four-band structure as the pulse duration increases. Our analysis shows that the evolution of these band structures originates from the pulse-duration-dependent multiple ionization bursts of the second electron. These band structures unambiguously indicate the subcycle electron emission in SDI.

© 2015 Optical Society of America

OCIS codes: (020.4180) Multiphoton processes; (260.3230) Ionization; (270.6620) Strong-field processes.

References and links

1. B. Walker, B. Sheehy, L. F. Dimauro, P. Agostini, K. J. Schafer, and K. C. Kulander, "Precision measurement of strong field double ionization of helium," Phys. Rev. Lett. **73,** 1227–1230 (1994).
2. J. S. Parker, B. J. S. Doherty, K. T. Taylor, K. D. Schultz, C. I. Blaga, and L. F. DiMauro, "High-energy cutoff in the spectrum of strong-field nonsequential double ionization," Phys. Rev. Lett. **96,** 133001 (2006).
3. Y. Zhou, Q. Liao, Q. Zhang, W. Hong, and P. Lu,"Controlling nonsequential double ionization via two-color few-cycle pulses," Opt. Express **18,** 632–638 (2010).
4. Q. Liao, Y. Zhou, C. Huang, and P. Lu, "Multiphoton Rabi oscillations of correlated electrons in strong-field nonsequential double ionization," New J. Phys. **14,** 013001 (2012).
5. S. Baier and A. Becker, "Nonsequential double ionization of the hydrogen molecule: Dependence on molecular alignment," Phys. Rev. A **78,** 013409 (2008).
6. L. Zhang, X. Xie, S. Roither, Y. Zhou, P. Lu, D. Kartashov, M. Schöffler, D. Shafir, P. B. Corkum, A. Baltuška, A. Staudte, and M. Kitzler, "Subcycle control of electron-electron correlation in double ionization," Phys. Rev. Lett. **112,** 193002 (2014).
7. Y. Zhou, Q. Liao, and P. Lu,"Asymmetric electron energy sharing in strong-field double ionization of helium," Phys. Rev. A **82,** 053402 (2010).
8. V. V. Suran and I. P. Zapesochnyi, "Observation of Sr^{2+} in multiple-photon ionization of strontium," Sov. Tech. Phys. Lett. **1,** 420 (1975)
9. A. L'Huillier, L. A. Lompre, G. Mainfray, and C. Manus, "Multiply charged ions formed by multiphoton absorption processes in the continuum," Phys. Rev. Lett. **48,** 1814–1817 (1982).
10. C. M. Maharjan, A. S. Alnaser, X. M. Tong, B. Ulrich, P. Ranitovic, S. Ghimire, Z. Chang, I. V. Litvinyuk, and C. L. Cocke, "Momentum imaging of doubly charged ions of Ne and Ar in the sequential ionization region," Phys. Rev. A **72,** 041403(R) (2005).
11. A. N. Pfeiffer, C. Cirelli, M. Smolarski, R. Döner, and U. Keller, "Timing the release in sequential double ionization," Nature Phys. **7,** 428–433 (2011).

#238098 - $15.00 USD Received 15 Apr 2015; revised 1 Jun 2015; accepted 2 Jun 2015; published 5 Jun 2015
© 2015 OSA

12. A. N. Pfeiffer, C. Cirelli, M. Smolarski, X. Wang, J. H. Eberly, R. Döner, and U. Keller, "Breakdown of the independent electron approximation in sequential double ionization," New J. Phys. **13,** 093008 (2011).
13. Y. Zhou, C. Huang, Q. Liao, and P. Lu, "Classical simulations including electron correlations for sequential double ionization," Phys. Rev. Lett. **109,** 053004 (2012).
14. P. B. Corkum, "Plasma perspective on strong field multiphoton ionization," Phys. Rev. Lett. **71,** 1994–1997 (1993).
15. Th. Weber, H. Giessen, M. Weckenbrock, G. Urbasch, A. Staudte, L. Spielberger, O. Jagutzki, V. Mergel, M. Vollmer, and R. Dörner, "Correlated electron emission in multiphoton double ionization," Nature **405,** 658–661 (2000).
16. M. Weckenbrock, D. Zeidler, A. Staudte, Th. Weber, M. Schöffler, M. Meckel, S. Kammer, M. Smolarski, O. Jagutzki, V. R. Bhardwaj, D. M. Rayner, D. M. Villeneuve, P. B. Corkum, and R. Dörner, "Fully differential rates for femtosecond multiphoton double ionization of neon," Phys. Rev. Lett. **92,** 213002 (2004).
17. R. Moshammer, B. Feuerstein, W. Schmitt, A. Dorn, C. D. Schröter, J. Ullrich, H. Rottke, C. Trump, M. Wittmann, G. Korn, K. Hoffmann, and W. Sandner, "Momentum distributions of Ne^{n+} ions created by an intense ultrashort laser pulse," Phys. Rev. Lett. **84,** 447–450 (2000).
18. A. Staudte, C. Ruiz, M. Schöffler, S. Schössler, D. Zeidler, Th. Weber, M. Meckel, D. M. Villeneuve, P. B. Corkum, A. Becker, and R. Dörner, "Binary and recoil collisions in strong field double ionization of Helium," Phys. Rev. Lett. **99,** 263002 (2007).
19. Y. Liu, S. Tschuch, A. Rudenko, M. Dürr, M. Siegel, U. Morgner, R. Moshammer, and J. Ullrich, "Strong-field double ionization of Ar below the recollision threshold," Phys. Rev. Lett. **101,** 053001 (2008).
20. W. Becker, X. Liu, P. J. Ho, and J. H. Eberly, "Theories of photoelectron correlation in laser-driven multiple atomic ionization," Rev. Mod. Phys. **84,** 1011–1042 (2012).
21. Y. Zhou, Q. Liao, and P. Lu, "Mechanism for high-energy electrons in nonsequential double ionization below the recollision-excitation threshold," Phys. Rev. A **80,** 023412 (2009).
22. J. Chen, J. Liu, L. B. Fu, and W. M. Zheng, "Interpretation of momentum distribution of recoil ions from laser-induced nonsequential double ionization by semiclassical rescattering model," Phys. Rev. A **63,** 011404(R) (2000).
23. A. Tong, Y. Zhou, C. Huang, and P. Lu, "Electron dynamics of molecular double ionization by circularly polarized laser pulses," J. Chem. Phys. **139,** 074308 (2013).
24. Y. Zhou, Q. Zhang, C. Huang, and P. Lu, "Classical description of strong-field double ionization by elliptical laser pulses," Phys. Rev. A **86,** 043427 (2012).
25. X. Wang and J. H. Eberly, "Classical theory of high-field atomic ionization using elliptical polarization," Phys. Rev. A **86,** 013421 (2012).
26. P. Wustelt, M. Möller, T. Rathje, A. M. Sayler, T. Stöhlker, and G. G. Paulus, "Momentum-resolved study of the saturation intensity in multiple ionization," Phys. Rev. A **91,** 031401 (2015).
27. B. Bergues, M. Kbel1, N. G. Johnson, B. Fischer, N. Camus, K. J. Betsch, O. Herrwerth, A. Senftleben, A. M. Sayler, T. Rathje, T. Pfeifer, I. Ben-Itzhak, R. R. Jones, G. G. Paulus, F. Krausz, R. Moshammer, J. Ullrich, and M. F. Kling, "Attosecond tracing of correlated electron-emission in non-sequential double ionization," Nat. Commun. **3,** 813 (2012).
28. C. L. Kirschbaum and L. Wilets, "Classical many-body model for atomic collisions incorporating the Heisenberg and Pauli principles," Phys. Rev. A **21,** 834–841 (1980).
29. D. Zajfman and D. Maor, "Heisenberg core in classical-trajectory monte carlo calculations of ionization and charge exchange," Phys. Rev. Lett. **56,** 320–323 (1986).
30. J. S. Cohen, "Quasiclassical-trajectory Monte Carlo methods for collisions with two-electron atoms," Phys. Rev. A **54,** 573–586 (1996).
31. W. A. Beck and L. Wilets, "Semiclassical description of proton stopping by atomic and molecular targets," Phys. Rev. A **55,** 2821–2829 (1997).
32. P. B. Lerner, K. J. LaGattuta, and J. S. Cohen, "Ionization of helium by a short pulse of radiation: A Fermi molecular-dynamics calculation," Phys. Rev. A **49,** R12–R15 (1994).
33. E. Lötstedt, T. Kato, and K. Yamanouchi, "Classical dynamics of laser-driven D_3^+," Phys. Rev. Lett. **106,** 203001 (2011).
34. C. Huang, Z. Li, Y. Zhou, Q. Tang, Q. Liao, and P. Lu, "Classical simulations of electron emissions from H_2^+ by circularly polarized laser pulses," Opt. Express **20,** 11700 (2012).
35. Y. Zhou, C. Huang, and P. Lu, "Revealing the multi-electron effects in sequential double ionization using classical simulations," Opt. Express **20,** 20201 (2012).
36. S. L. Haan, L. Breen, A. Karim, and J. H. Eberly, "Variable time lag and backward ejection in full-dimensional analysis of strong-field double ionization," Phys. Rev. Lett. **97,** 103008 (2006).
37. Phay J. Ho, R. Panfili, S. L. Haan, and J. H. Eberly, "Nonsequential double ionization as a completely classical photoelectric effect," Phys. Rev. Lett.**94,** 093002 (2005).
38. Y. Zhou, C. Huang, A. Tong, Q. Liao, and P. Lu, "Correlated electron dynamics in nonsequential double ionization by orthogonal two-color laser pulses," Opt. Express **19,** 2301–2308 (2011).
39. C. Huang, Y. Zhou, Q. Zhang, and P. Lu, "Contribution of recollision ionization to the cross-shaped structure in

#238098 - $15.00 USD Received 15 Apr 2015; revised 1 Jun 2015; accepted 2 Jun 2015; published 5 Jun 2015
© 2015 OSA

nonsequential double ionization," Opt. Express **21,** 11382–11390 (2013).
40. M. S. Schöffler, X. Xie, S. Roither, D. Kartashov, A. Baltuska, and M. Kitzler, "Strong field double ionization of Helium with ultra-short phase stabilized circularly polarized laser pulses," J. Phys: Conf. Ser. **488,** 032010 (2014).

1. Introduction

Double ionization (DI) is one of the most fundamental and important process in intense laser-atom interactions. Generally, DI can occur through two different pathways, nonsequential double ionization (NSDI) [1-9] and sequential double ionization (SDI) [10-13]. In NSDI, the second electron is ionized by the recollision of the first electron [14]. Because of the recollision, the two electrons in NSDI exhibit a highly correlated behavior. During the past decades NSDI has been extensively investigated both theoretically and experimentally [15-23]. For SDI, the two electrons are released sequentially by the laser field. The process of SDI is relatively simpler and less attention has been paid during the past decades. However, SDI by elliptically polarized laser pulse can provide much ionization information that is unreachable in NSDI. For example, by measuring the ion momentum from SDI in the elliptically polarized pulses, people observed the sequential nature of the emission process of the two electrons [10]. In recent years, SDI in the elliptical laser fields has attracted more and more attentions. For instances, a recent experiment has systematically investigated SDI of Ar by elliptical laser fields over a wide range of laser intensity and the times of the ionization bursts for both electrons as a function of laser intensity are extracted [11]. In that experiment, it was shown that, the momentum distribution of the doubly charged ion in the laser polarization plane exhibited a four-band structure at high laser intensities and it evolved into a three-band structure as the laser intensity decreased. With the classical ensemble method, this behavior has been well reproduced and the sequential nature of double ionization has been intuitively shown [13, 24]. It has been demonstrated that these band structures are closely related to the launching time of the ionization bursts of the two electrons. Classical calculations also shown that for multiple ionization the corresponding momentum spectrum of the ions will exhibit more bands. For example, it was predicted that the ion momentum spectrum will exhibit eight bands in sequential triple ionization [25]. In a very recent experiment for triple ionization of Ne^+, a six-band structure in ion momentum spectra was observed [26]. From these structures, the saturate ionization intensity as well as the ionization time for each ionization step are successfully extracted. In all of these experiments, only one ionization burst for each ionization step was obtained. Usually, the ionization of each electron lasts over a range of time longer than one optical cycle. In the elliptical laser field, the most likely ionization scenario is that in each half cycle there is one subcycle ionization burst launching at the time when the transient electric field points along the major elliptical axis. Thus, the experimentally extracted ionization bursts for each ionization step should contain many subcycle ionization bursts. However, these subcycle ionization bursts have not yet been resolved in experiment on SDI. This may be due to the laser parameters (such as laser intensity, pulse duration) in these experiments are not suitable for this observation. We mention that in NSDI the subcycle electron emission after recollision has been well explored with the single-cycle pulses [27].

In this paper, we theoretically investigate SDI by the elliptical laser fields at intensity well in the over-barrier ionization region. Our calculations predict that depending on the pulse duration, the spectra of doubly charged ion exhibit different number of bands. For the very short pulse duration, the spectrum shows a two-band structure and it evolves into a four-band structure as the duration increases. When the pulse duration increases further, an obvious six-band structure appears and finally it evolves into the previously observed four-band structure. Our analysis shows that these phenomena are the manifestation of the subcycle ionization bursts of

#238098 - $15.00 USD Received 15 Apr 2015; revised 1 Jun 2015; accepted 2 Jun 2015; published 5 Jun 2015
© 2015 OSA

the second electrons during the laser pulses. Our calculations indicate that the subcycle ionization emission in SDI can be observed by properly choosing the laser parameters.

2. The classical ensemble model

In this paper, we employ the purely classical model, Heisenberg-core potential model (HPCM) [13], to study SDI at over-barrier ionization region. The Heisenberg-core potential was originally introduced by Kirschbaum and Wilets [28] and it was later widely used in atomic and molecular collisions [29-31], and very recently its application has been extended to strong-field ionization [32-35]. In HPCM, the Heisenberg-core potential was employed to avoid autoionization of the classical two-electron system and to match the ionization potentials of the model atoms to the real systems [13]. The accuracy of this Heisenberg-core potential model in strong field double ionization has been confirmed in recent studies [13, 24], where the experimentally measured momentum spectra of doubly charged ion in SDI as well as the ionization times of both electrons are qualitatively reproduced by this classical model. Thus, we employ this model to study SDI by elliptical laser fields with different pulse durations.

In HPCM, the Hamiltonian of the two-electron system is written as [13] (atomic units are used throughout this paper unless stated otherwise)

$$H = \frac{1}{|\mathbf{r}_1 - \mathbf{r}_2|} + \sum_{i=1,2} [-\frac{1}{r_i} + \frac{p_i^2}{2} + V_H(r_i, p_i)] + (\mathbf{r}_1 + \mathbf{r}_2) \cdot \mathbf{E}(t), \tag{1}$$

where i=1,2 is the electron label and r_i, p_i are the position and canonical momentum of the i_{th} electron, respectively. $\mathbf{E}(t)$ is an elliptically polarized electric field, which is written as:

$$\mathbf{E}(t) = f(t)[\frac{1}{\sqrt{\varepsilon^2+1}} \cos(\omega t + \phi)\hat{\mathbf{x}} + \frac{\varepsilon}{\sqrt{\varepsilon^2+1}} \sin(\omega t + \phi)\hat{\mathbf{y}}], \tag{2}$$

where $f(t) = E_0 \sin^2(\frac{\pi t}{NT})$ is the pulse envelope. $E_0, \omega, \varepsilon, \phi, T, N$ are amplitude, frequency, ellipticity, carrier-envelope phase (CEP), period and period number of the laser pulse respectively. $V_H(r_i, p_i)$ is the Heisenberg-core potential, which is expressed as [13, 28]

$$V_H(r_i, p_i) = \frac{\xi^2}{4\alpha r_i^2} \exp\left\{\alpha[1 - (\frac{r_i p_i}{\xi})^4]\right\}, \tag{3}$$

where the parameter α indicates the rigidity of the Heisenberg core. For a given α, the parameter ξ is chosen to match the second ionization potential of the target [13]. For Ar, the rigidity parameter α is set to be 2, then ξ is set to make the minimum of the one-electron Hamilton $[H_1 = -\frac{2}{r_1} + \frac{p_1^2}{2} + V_H(r_1, p_1)]$ equal to the second ionization potential of Ar (-1.01 a.u.) and we obtain ξ=1.225. The ground-state energy of Ar is set to the sum of the first and the second ionization potential (-1.59 a.u.) and the initial distributions of the ground-state atom in the phase space are obtained with the approach in the soft-core potential classical model [36-39].

Once the initial state is obtained, the laser is turned on. In our calculations, the intensity of the laser field is 6.0 PW/cm^2. The wavelength and the ellipticity are is 800 nm and 0.75, respectively. The pulse duration N ranges from 4 to 14 optical cycle. The evolution of the two-electron system is determined by the equations:

$$\frac{d\mathbf{r}_i}{dt} = \frac{\partial H}{\partial \mathbf{p}_i}, \frac{d\mathbf{p}_i}{dt} = -\frac{\partial H}{\partial \mathbf{r}_i}. \tag{4}$$

At the end of the laser pulse, we examine the DI yields. We define that the electron is ionized if its final energy is positive. Double ionized is defined when both electrons possess positive

#238098 - $15.00 USD Received 15 Apr 2015; revised 1 Jun 2015; accepted 2 Jun 2015; published 5 Jun 2015
© 2015 OSA

energy at the end of the pulse. For the present laser parameters, almost all of the DIs are SDI since recollision is completely suppressed because of large ellipticity.

3. Results and discussion

In Fig. 1, we display the ion momentum distributions in the polarization plane for SDI of Ar by elliptically polarized laser pulses with period number N ranging from 4 to 14. The ion momentum of Ar^{2+} is obtained by the negative sum of the two electron momentum vector, i.e.$p_{x,ion} = -(p_{x,e1} + p_{x,e2})$, because the momentum of the absorbed photons is negligibly small. In these calculations, CEP is random for each atom, corresponding to a phase-unlocked experiment. Figure 1 shows that the ion momentum distributions in the direction of the minor elliptical axis ($\hat{\mathbf{y}}$ axis) exhibit band structures and the numbers of the bands depend on the laser duration. For the pulse duration N=4, the distribution shows two bands. When the pulse duration increases to N=6, two more bands appear though it is relatively weaker. For N=8, the outer two bands become more obvious. Between the inner and outer bands, two more bands appear. These two bands become very strong at N=10 and the spectrum exhibits a very clear six-band structure. When the pulse duration increases further, the two inner bands disappear gradually and finally only four bands are visible for the case N=14.

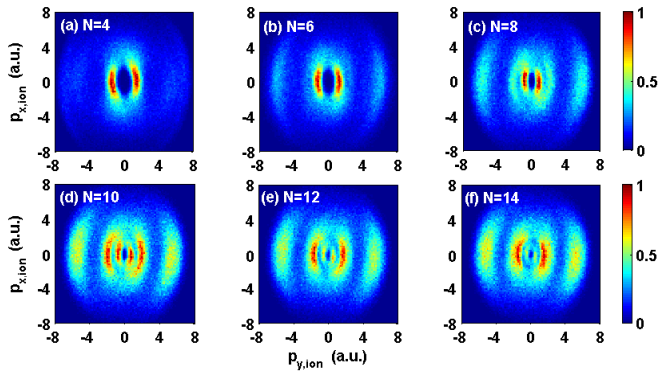

Fig. 1. Ion momentum distributions in the laser polarization plane for different pulse durations. The intensity of the laser pulses is 6.0 PW/cm^2, the wavelength is 800 nm, and the ellipticity is ε=0.75. The CEP is randomly chosen for each trajectory. The ensembles are 400000.

This change of ion momentum distributions with pulse duration can be more clearly seen in Fig. 2, where the ion momentum distributions in the direction of the minor elliptical axis ($\hat{\mathbf{y}}$ axis) are shown (obtained by integrating the distributions of Fig. 1 over the $p_{x,ion}$ axis). For the pulse duration N=4, the spectrum exhibits two peaks, which are labeled as P_1. As the pulse duration increases, two outer peaks (P_2) become very clear, and two more peaks (P_3) between P_1 and P_2 appear. At N=10, the spectrum exhibits a very clear six-peak structure. As the pulse duration increases further, the peaks P_3 become stronger while the peaks P_1 become weaker. Finally, P_1 peaks almost disappear and only peaks P_2 and P_3 remain visible at N=14. Additionally, one can see that the separation between the two P_1 peaks decreases when the pulse duration increases.

The results above are very different from the previous observations [10, 11], where it has been shown that the ion momentum distribution from SDI exhibits the three-band structures at low laser intensities and the four-band structure at high laser intensities. In our calculations of high laser intensity, the ion momentum distributions evolve from the two-band structure to the

#238098 - $15.00 USD Received 15 Apr 2015; revised 1 Jun 2015; accepted 2 Jun 2015; published 5 Jun 2015
© 2015 OSA

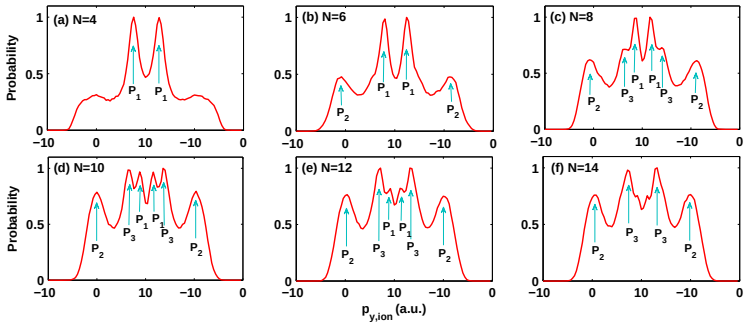

Fig. 2. Ion momentum distributions along the minor elliptical axis ($\hat{\mathbf{y}}$ axis) for different pulse durations. The laser parameters are the same as those in Fig. 1.

four-band, six-band structure and finally to the previously obtained four-band structure as the pulse duration increases. In order to understand the physical process for this pulse duration dependence of ion momentum distributions, we recalculated SDI with the same laser parameters as those in Fig. 1 but with fixed CEP ϕ=0. The results are shown in Fig. 3. For the short pulses, the distributions are asymmetric. For example, at the pulse duration N=4, only one band appears at negative momentum and the peak with positive momentum is absent. This is due to the asymmetry of the electric field of the short pulses. The other band will appear for other CEPs. This is the same situation for pulse durations N=6 to N=10. For longer pulses, the distributions no longer depend on CEP and they become symmetric gradually.

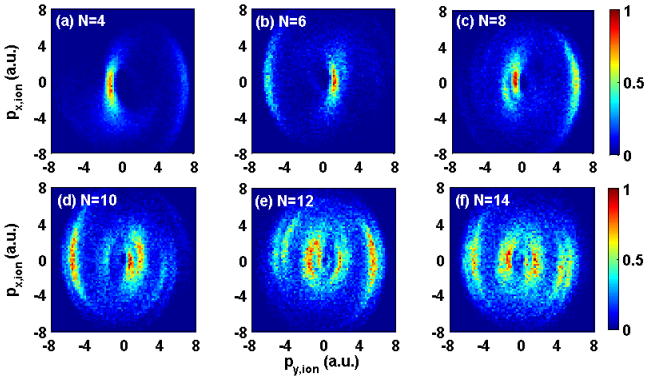

Fig. 3. Ion momentum distributions in the laser polarization plane for different pulse durations with $\phi = 0$. Other parameters are the same as those in Fig. 1.

It has been demonstrated that these band structures contain information about the sequential release of the electrons, and the ionization times can be extracted from these structures if the ionization laser field is known. In other words, these structures are related to the ionization times of electrons. In order to reveal the correspondence between the multiple-band structures and the ionization times, we extracted the ionization times of the two electrons. The ionization times can be extracted either from the ion momentum distributions or the electron momentum distributions [25]. Here, we extract them from the electron momentum distributions, with the procedure similar to that in [11, 13]. The right column of Fig. 4 shows electron correlation spectra for the scaled radial momentum p_r' with $\phi = 0$, where p_r' is defined as [11]

#238098 - $15.00 USD Received 15 Apr 2015; revised 1 Jun 2015; accepted 2 Jun 2015; published 5 Jun 2015
© 2015 OSA

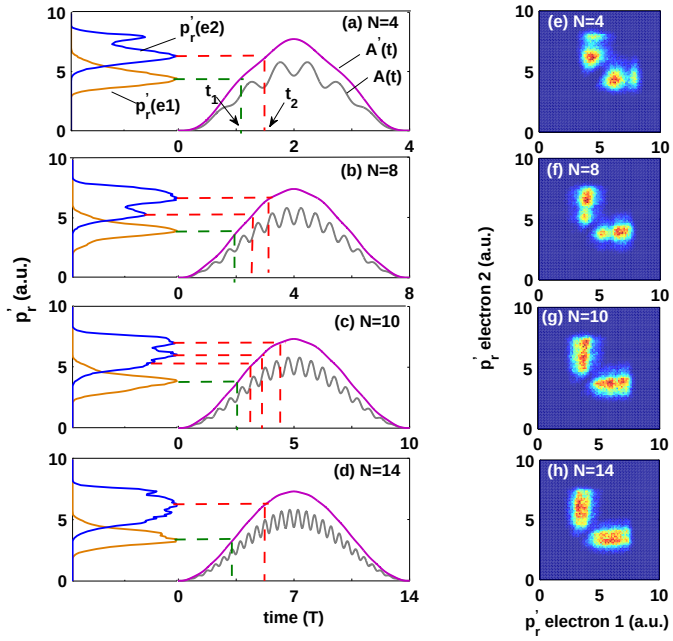

Fig. 4. (Left) The procedure of extracting ionization time from electron momentum spectrum. The brown and blue curves in left side are the scaled radial momentum distributions of the first and the second electrons, respectively. The grey curves show the vector potential $\mathrm{A}(\mathrm{t})$ where $\mathrm{A}(\mathrm{t}) = [\mathrm{A_x}(\mathrm{t})^2 + \mathrm{A_y}(\mathrm{t})^2]^{1/2}$. The magenta curves denote the scaled vector potential $\mathrm{A}'(\mathrm{t})$. The dashed lines are added to guide eyes and show the relation between the electron final momentum and ionization times. (Right) The electron correlation spectra for the scaled radial momentum with $\phi = 0$.

$$p'_{r,i} = [(\varepsilon^2+1)p_{x,i}^2 + ((\varepsilon^2+1)/\varepsilon^2)p_{y,i}^2]^{1/2}, \tag{5}$$

where i=1,2 is the electron label. With this scale, the radial momentum is an injective function of time with the condition that the electrons are ionized before the peak of the pulses [11]. These spectra are symmetric with respect to the diagonal because we do not distinguish the first and the second electrons here. For high laser intensity in our calculations, both electrons are ionized within the rising edge of the laser pulse, and thus the electrons ionized earlier will achieve smaller final momentum. Therefore, we can distinguish which electron is ionized first based on the final momentum. In the following, we denote the electron with smaller final momentum (thus ionized first) as the first electron and the other electron as the second electron. Projecting the peak positions of the scaled radial momenta of the first and the second electrons to the scaled vector potential of the laser field, the ionization times of both electrons are extracted, as shown in the left column of Fig. 4. The scaled vector potential is expressed as:

$$\mathrm{A}'(\mathrm{t}) = [(\varepsilon^2+1)\mathrm{A_x}(\mathrm{t})^2 + ((\varepsilon^2+1)/\varepsilon^2)\mathrm{A_y}(\mathrm{t})^2]^{1/2}, \tag{6}$$

where $\mathrm{A_x}, \mathrm{A_y}$ are the vector potential components along $\hat{\mathbf{x}}$ and $\hat{\mathbf{y}}$ axis, respectively. Here, the extraction of the ionization time is based on two approximations the electron is ionized with zero initial momentum and after ionization the interaction between the electron and ion is negligible.

#238098 - $15.00 USD Received 15 Apr 2015; revised 1 Jun 2015; accepted 2 Jun 2015; published 5 Jun 2015
© 2015 OSA

Figure 4 shows that for the first electron, the ionization time is confined within half cycle. However, for the second electron, the ionization time depends on the pulse duration. For N=4, the ionization time is mainly around the next half cycle of the first ionization. For these events, the two electrons emit into the opposite directions and thus the value of the ion momentum is small, resulting in the two P_1 peaks in Fig. 2. When the pulse duration increases to N=8, another ionization burst at one laser cycle later after the first ionization becomes very strong. For this ionization burst, the two electrons emit into the same direction and contribute to the two P_2 peaks in Fig. 2. When the pulse duration increases further, three ionization bursts for the second electron appear and correspondingly there are three pairs of peaks in the ion momentum spectra. For longer pulses, we could expect that there will be more ionization bursts for the second electron. However, for the long pulses the final momentum difference of the electrons ionized at adjacent cycles is very small and thus the multiple ionization bursts of the ionization time are unresolvable from the ion and electron momentum spectra, as shown in Fig. 4(d).

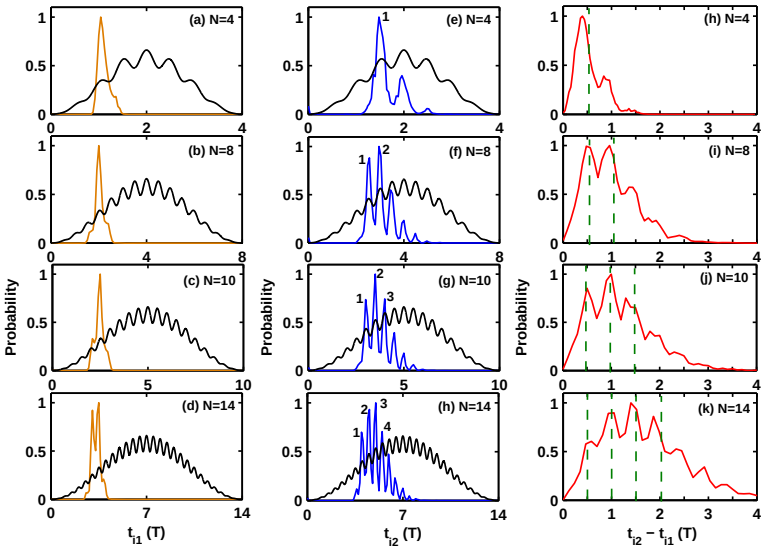

Fig. 5. Distributions of the ionization time for the first electron(t_{i1}) [the first column] and the second electron(t_{i2}) [the second column]. The third column shows the distribution for the time delay between the second and the first ionizations ($t_{i2} - t_{i1}$). The green dashed lines in the third column represent delay time of integer multiples of half laser cycle, which are added to guide eyes. The CEP is $\phi = 0$ and the pulse durations are denoted in the each plot.

The analysis above shows that the multiple-band structure is related to the ionization times of the electrons. Thus, these band structures directly indicate the subcycle ionization bursts in SDI. Our classical method also allows us to trace the ionization times from the classical trajectories and confirm the analysis above. The ionization time is defined as the instant when the energy of the electron becomes positive for the first time. In Fig. 5, with $\phi = 0$, we show the distributions of ionization times of the first and the second electrons by tracing the classical trajectories. As shown in the first column of Fig. 5, for the short pulse durations (N=4 to N=10), there is only one ionization burst for the first electrons, meaning that the first electron is completely ionized within half cycle at this high laser intensity. For the second electron, it is mainly ionized within half cycle just after the first ionization at N=4 [Fig. 5(e)]. As the pulse duration increases, more ionization bursts denoted by “2” and “3” appear. For the long pulse N=14, there are two ion-

#238098 - $15.00 USD Received 15 Apr 2015; revised 1 Jun 2015; accepted 2 Jun 2015; published 5 Jun 2015
© 2015 OSA

ization bursts for the first electron and many bursts for the second electrons. These results from our trajectory tracing are consistent with those obtained from the calculated electron momentum spectra (Fig. 4), confirming the reliability of reading ionization time from ion and electron momentum distributions. Thus, the multiple-band structures in the ion momentum distributions definitely indicate the subcycle ionization bursts in SDI.

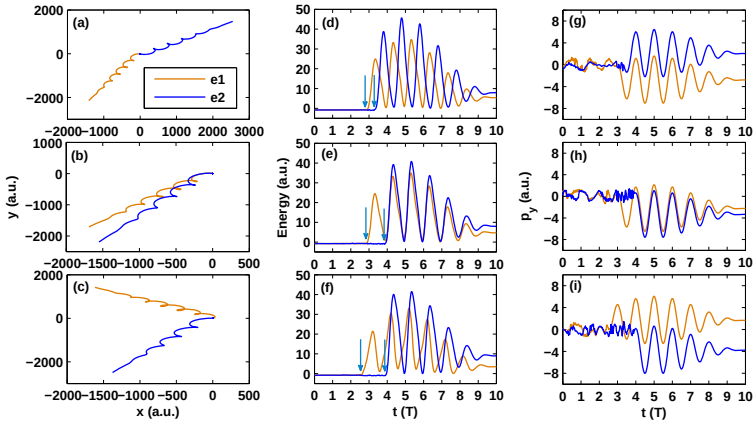

Fig. 6. Three sample SDI trajectories for pulse duration N=10. The first, second and third columns display the trajectories in the laser polarization plane, the time evolution of the energy and the time evolution of the momentum p_y, respectively. The ionization time of the two electrons are indicated by the arrows in the second column.

The third column of Fig. 5 shows the distributions of time delay between the first and second ionizations. The two electrons will emit into the same direction when their ionization time delay is even multiples of half cycle and into the opposite directions when it is odd multiples of half cycle. For the events where the second electron ionized within burst "2" the two electrons emit into the same direction, and the corresponding ion momentum distribution is located at peaks P_2 of Fig. 2. Similarly, the ionization bursts "1" and "3" result in the inner peaks P_1 and P_3 of Fig. 2. The separation of the two P_1 peaks is determined by the momentum difference of the two electrons. For this pair of peaks, the ionization time delay between the two electrons is half cycle. Assuming that the initial momentum at ionization is negligible, the final momenta of the electrons are $\mathbf{p}_{ei} = \mathbf{A}(t_i) = -\int_{t_i}^{+\infty} \mathbf{E}(t)\,dt$, where t_i is the ionization time of the i_{th} electron and $\mathbf{E}$(t) is the electric field. Thus, for a fixed laser intensity, the momentum difference decreases as the pulse duration increases. Consequently, the separation of the two P_1 peaks decreases with the increasing pulse duration [Fig. 2].

To give a more intuitive picture of the SDI process, we show three illustrative trajectories in Fig. 6. The first, second and third columns display the trajectories in the laser polarization plane, the time evolution of the energy and the time evolution of the momentum p_y, respectively. The ionization time of the two electrons are indicated by the arrows in the second column. For the first trajectory (the upper line) the time delay between the two ionization is about half cycle and the two electrons achieve final momentum p_y with opposite directions. For the second trajectory (the middle line), the time delay of ionization is one cycle and two electrons acquire final momentum p_y with the same direction. For the third trajectory (the bottom line), the time delay of ionization is 3 half cycles and again the directions of the final momentum of the two electrons are opposite.

We note that in our calculations we did not considered the focal volume effect of the laser pulse. When this effect is considered, the bands in the momentum spectra will be broaden

#238098 - $15.00 USD Received 15 Apr 2015; revised 1 Jun 2015; accepted 2 Jun 2015; published 5 Jun 2015
© 2015 OSA

and thus the multiple-band structure will be obscured. With longer wavelength, the separation between the bands will become larger and thus it will be easier to observe these multi-band structures in experiment.

4. Conclusion

In conclusion, we have investigated SDI of Ar by elliptically polarized laser pulse with the Heisenberg-core potential classical model. We resolved the multiple-band structure in the ion momentum spectra. This structure originates from the multiple ionization bursts of the second electrons and it directly reveals the subcycle electron emission nature of SDI in the elliptical laser field. Experimentally, these subcycle multiple ionization bursts can be observed using high-intensity (so that both electrons are ionized during the rising edge of pulse) laser pulses with short pulse durations, and longer wavelength will be more favorable. Recently this multiple-band structure has been experimentally observed for SDI of Helium by intense few-cycle laser pulses [40].

Acknowledgment

This work was supported by the National Natural Science Foundation of China under Grant No. 61405064, 11404105, 11234004, Chinese Postdoctoral Science Foundation under Grant No. 2014M550388, and the Natural Science Foundation of Hubei Province under Grant No. 2013CFB015.

#238098 - $15.00 USD Received 15 Apr 2015; revised 1 Jun 2015; accepted 2 Jun 2015; published 5 Jun 2015
© 2015 OSA